Free-boundary dynamics in elastoplastic amorphous solids: The circular hole problem

Eran Bouchbinder,[1] J. S. Langer,[2] Ting-Shek Lo,[1] and Itamar Procaccia[1]
[1]*Department of Chemical Physics, The Weizmann Institute of Science, Rehovot 76100, Israel*
[2]*Department of Physics, University of California, Santa Barbara, California, USA*
(Received 25 December 2006; published 28 August 2007)

We develop an athermal shear-transformation-zone (STZ) theory of plastic deformation in spatially inhomogeneous, amorphous solids. Our ultimate goal is to describe the dynamics of the boundaries of voids or cracks in such systems when they are subjected to remote, time-dependent tractions. The theory is illustrated here for the case of a circular hole in an infinite two-dimensional plate, a highly symmetric situation that allows us to solve much of the problem analytically. In spite of its special symmetry, this example contains many general features of systems in which stress is concentrated near free boundaries and deforms them irreversibly. We depart from conventional treatments of such problems in two ways. First, the STZ analysis allows us to keep track of spatially heterogeneous, internal state variables such as the effective disorder temperature, which determines plastic response to subsequent loading. Second, we subject the system to stress pulses of finite duration, and therefore are able to observe elastoplastic response during both loading and unloading. We compute the final deformations and residual stresses produced by these stress pulses. Looking toward more general applications of these results, we examine the possibility of constructing a boundary-layer theory that might be useful in less symmetric situations.

DOI: 10.1103/PhysRevE.76.026115 PACS number(s): 46.35.+z, 83.80.Ab

I. INTRODUCTION

The aim of this paper is to develop a theoretical description of the way in which the boundaries of voids in amorphous solids move under the influence of external loads. An obvious example is dynamic fracture. The evolution of cracks is traditionally described by linear elasticity. However, elasticity by itself does not provide a dynamical theory of crack motion but, instead, uses criteria such as an energy balance to provide bounds on the velocities of straight cracks [1]. This approach was challenged by one of us in Ref. [2]. More recently, starting with closely related ideas, it was shown in Ref. [3] that taking into account the dynamic degrees of freedom near a moving crack tip resolves various inconsistencies in traditional theories of linear elastic fracture mechanics. Nevertheless, the theoretical approach of Ref. [3] is far from complete; it is still not an accurate and internally self-consistent description of free-boundary motion.

We do not deal with the actual dynamics of cracks in this paper. Rather, we apply the shear-transformation-zone (STZ) theory developed in two recent papers [4,5] to the dynamics of a circular hole in an infinite medium. We have chosen this highly symmetric example in order to simplify the tensorial character of the theory, and to help in developing analytic methods that may remain applicable in less symmetric situations. As we shall see, the solutions of the circle problem provide a wealth of information about the ways in which stress concentrations near moving free boundaries induce plastic deformation.

The STZ approach that we employ here is based on recent developments in the theory of dynamic elastoplastic deformation of amorphous materials at low temperatures [4]. The theory was applied to a homogenous situation in [4] and the results were compared to recent numerical simulations in [5]. The STZ theory, originally proposed in Refs. [6,7], deviates from conventional approaches [8] by focusing on the nature of the microscopic mechanisms for plastic deformation in amorphous media. These mechanisms are incorporated into the macroscopic description by internal state fields. An important observation is that the plastic strain itself cannot be one of these fields. For that to be true, the material would somehow have to encode information about its entire history of deformation starting from some reference state. This is not possible. More realistically, the memory of prior deformations, and the rate at which that memory is lost, must be encoded in the internal state variables and their equations of motion. The identification of the physically appropriate microscopic variables is based here on the notion that STZ's are sparsely distributed, localized clusters of molecules that are especially susceptible to rearrangement in response to applied stresses. To take the STZ's and their role in the dynamics into account, one introduces a scalar field that describes the density of STZ's and a tensorial one that describes their orientation. Equations of motion for both the plastic strain rate and these internal state fields are obtained by assuming that STZ's change orientation (deform by finite amounts) at rates that depend on the stress. In addition, STZ's are created and annihilated at rates proportional to the rate at which the energy of plastic deformation is dissipated [7].

An earlier STZ analysis of the circle problem [9] was based on a "quasilinear" version of the theory that used a conveniently truncated form of the transition rates [6,7]. This relatively simple theory captured linear viscoelasticity at small stresses, finite viscoplasticity at intermediate stresses, and unbounded plastic deformation at large stresses as a result of an exchange of dynamic stability between jammed (nondeforming) and unjammed (deforming) states of the system. Some memory effects were also described successfully. The quasilinear theory, however, had serious limitations; and therefore we base the present analysis on the recent version of STZ theory [4] that starts with more physically realistic assumptions. In Ref. [4], it was argued that the defining fea-

ture of a system at low temperatures is the constraint that, because thermal activation of STZ transitions is negligible or nonexistent, each molecular rearrangement occurs in response to an external driving force. No motion occurs in the absence of such a force, and no rearrangement moves in opposition to the direction of that force. In addition, this version of STZ theory includes the possibility that STZ's occur in many different types and with a range of different transition thresholds.

The problem of dynamic hole growth in plastically deforming solids has a long history. For example, see early work by McClintock [10], Rice and Tracey [11], Carroll and Holt [12], Johnson [13], and Bodner and Partom [14]. Our present analysis goes beyond this earlier work, and beyond the results presented in Ref. [9] in many respects; specifically, the following.

(1) We employ here the fully nonlinear, athermal theory described in Ref. [4], and therefore automatically include hardening and rate-dependent effects that were missing in all the early work cited above.

(2) The material time derivatives are expressed in a proper Eulerian formulation and the theory is consistent with all relevant conservation laws and symmetries.

(3) The calculation described here takes into account the dynamics of the density of STZ's via an effective-temperature formulation, a feature that is shown in Refs. [4,5] to be essential for self-consistency in these theories.

(4) The focus here is on the transient growth regime that is relevant to dynamic situations such as fracture. Instead of considering only constant loads, we look at the elastoplastic response to a stress pulse, and study the behavior during both loading and subsequent unloading.

(5) We develop a boundary layer theory that provides a useful approximation for the exact numerical solution.

The organization of this paper is as follows. In Sec. II we write the equations of motion and the boundary conditions for a circular hole in an infinite sheet of material subjected to a uniform radial stress at infinity. In Sec. III, we review the elements of the STZ theory that are needed for this problem and specialize to cases of interest here. Section IV contains discussions of the specific situations to be considered in more detail, starting with the two different loading schemes to be used, and then the simplifying assumption of elastic incompressibility. Our numerical results for both constant applied stress and two different stress pulses are presented in Sec. V. Section VI is devoted to the development of a boundary layer approximation and its comparison with the numerical results. Finally, in Sec. VII, we offer a summary and further discussion. In the Appendix, we show how to compute the threshold for unbounded growth of the circular hole under constant remote loading.

II. EQUATIONS AND BOUNDARY CONDITIONS

A. Strain, stress, and rate of deformation

We start by writing the full set of equations for a general two-dimensional elastoplastic material. We define the total rate-of-deformation tensor

$$D_{ij}^{\mathrm{tot}} \equiv \frac{1}{2}\left(\frac{\partial v_i}{\partial x_j} + \frac{\partial v_j}{\partial x_i}\right), \tag{2.1}$$

where $\boldsymbol{v}(\boldsymbol{r},t)$ is the material velocity at the location $\boldsymbol{r}$ at time t. This type of Eulerian formulation has the advantage that it disposes of any reference state, allowing free discussion of small or large deformations. The price that we pay is that, in inhomogeneous situations, we need to employ the full material derivative for a tensor $\boldsymbol{A}$,

$$\frac{\mathcal{D}\boldsymbol{A}}{\mathcal{D}t} = \frac{\partial \boldsymbol{A}}{\partial t} + \boldsymbol{v}\cdot\boldsymbol{\nabla}\boldsymbol{A} + \boldsymbol{A}\cdot\boldsymbol{\omega} - \boldsymbol{\omega}\cdot\boldsymbol{A}, \tag{2.2}$$

where ω is the spin tensor

$$\omega_{ij} \equiv \frac{1}{2}\left(\frac{\partial v_i}{\partial x_j} - \frac{\partial v_j}{\partial x_i}\right). \tag{2.3}$$

For a scalar or vector quantity $\boldsymbol{A}$ the commutator with the spin tensor vanishes identically.

Plasticity is introduced by assuming that the total rate-of-deformation tensor can be written as a sum of elastic and plastic contributions

$$D_{ij}^{\mathrm{tot}} = \frac{\mathcal{D}\epsilon_{ij}^{\mathrm{el}}}{\mathcal{D}t} + D_{ij}^{\mathrm{pl}}. \tag{2.4}$$

On the face of it this looks similar to an innocent definition of D_{ij}^{pl}. We want, however, D_{ij}^{pl} to contain *all* the dissipative contributions to the dynamics. Such a linear superposition with this meaning in mind is only possible when the elastic deformations are small, see Ref. [15]. Once we assume small elastic deformations we can also use linear elasticity. The linear elastic strain tensor $\epsilon_{ij}^{\mathrm{el}}$ is related to the stress tensor whose general form is

$$\sigma_{ij} = -p\,\delta_{ij} + s_{ij}, \quad p = -\frac{1}{2}\sigma_{kk}. \tag{2.5}$$

The relation is

$$\epsilon_{ij}^{\mathrm{el}} = -\frac{p}{2K}\delta_{ij} + \frac{s_{ij}}{2\mu}, \tag{2.6}$$

where K and μ are the two-dimensional bulk and shear moduli respectively. s_{ij} is the deviatoric stress tensor and p is the pressure. The equations of acceleration and continuity are

$$\rho\frac{\mathcal{D}\boldsymbol{v}}{\mathcal{D}t} = \boldsymbol{\nabla}\cdot\sigma = -\boldsymbol{\nabla}p + \boldsymbol{\nabla}\cdot\boldsymbol{s}, \tag{2.7}$$

$$\frac{\mathcal{D}\rho}{\mathcal{D}t} = -\rho\,\boldsymbol{\nabla}\cdot\boldsymbol{v}. \tag{2.8}$$

Consider now an infinite two-dimensional amorphous material with a circular hole centered at the origin. The hole has radius R; and the system is loaded at infinity by a radial, uniform and possibly time-dependent stress $\sigma^{\infty}(t)$. For this configuration, the field of interest is the radial velocity $v_r(r,t)$, denoted here simply by $v(r,t)$. The nonvanishing components of D_{ij}^{tot} in Eq. (2.1) are

$$D_{rr}^{\mathrm{tot}} = \frac{\partial v}{\partial r}, \quad D_{\theta\theta}^{\mathrm{tot}} = \frac{v}{r}. \tag{2.9}$$

Note that D_{ij}^{tot} satisfies the compatibility relation

$$D_{rr}^{\mathrm{tot}} = \frac{\partial}{\partial r}(rD_{\theta\theta}^{\mathrm{tot}}). \tag{2.10}$$

The azimuthal velocity vanishes identically. Since the spin tensor vanishes identically in the circular symmetry, the material time derivative in Eq. (2.2) becomes

$$\frac{\mathcal{D}}{\mathcal{D}t} \equiv \frac{\partial}{\partial t} + v\frac{\partial}{\partial r}. \tag{2.11}$$

We now turn to the equations of motion (2.7). The symmetry of the problem implies that only the σ_{rr} and $\sigma_{\theta\theta}$ components of the stress tensor are nonvanishing. The tensor s_{ij} is diagonal, and thus we define the deviatoric stress s and the pressure p to be

$$p \equiv -\frac{1}{2}(\sigma_{\theta\theta} + \sigma_{rr}), \quad s \equiv s_{\theta\theta} = -s_{rr} = \frac{1}{2}(\sigma_{\theta\theta} - \sigma_{rr}). \tag{2.12}$$

Next we assume that the inertial term on the left-hand side of Eq. (2.7) is negligible and that density variations are also negligible; thus Eq. (2.8) is satisfied automatically, and Eqs. (2.7) reduce to a single force balance equation of the form [16]

$$\frac{\partial \sigma_{rr}}{\partial r} + \frac{\sigma_{rr} - \sigma_{\theta\theta}}{r} = 0, \tag{2.13}$$

which, with Eqs. (2.12), becomes

$$\frac{\partial p}{\partial r} = -\frac{1}{r^2}\frac{\partial}{\partial r}(r^2 s). \tag{2.14}$$

The hole edge is a free boundary, i.e., it is traction-free, and therefore the boundary conditions are

$$\sigma_{rr}(R,t) = -p(R,t) - s(R,t) = 0,$$

$$p \to -\sigma^{\infty}(t), \quad s \to 0 \text{ as } r \to \infty, \tag{2.15}$$

where $\sigma^{\infty}(t)$ is assumed to vary slowly enough that the omission of the inertial terms in Eq. (2.7) is still justified.

B. Introducing plasticity

Plasticity is introduced as in Eq. (2.4). According to Eq. (2.6), the components $\epsilon_{ij}^{\mathrm{el}}$ of the strain tensor satisfy

$$\epsilon_{rr}^{\mathrm{el}} = -\frac{p}{2K} - \frac{s}{2\mu},$$

$$\epsilon_{\theta\theta}^{\mathrm{el}} = -\frac{p}{2K} + \frac{s}{2\mu}. \tag{2.16}$$

The two-dimensional bulk modulus K is given by

$$K = \frac{\mu(1+\nu^*)}{1-\nu^*}, \tag{2.17}$$

where ν^* is the two-dimensional Poisson ratio. Unlike dislocation-caused plasticity in metals, plasticity in amorphous media may not be volume conserving. Nevertheless, for simplicity we take here the plastic rate-of-deformation tensor D_{ij}^{pl} to be traceless, implying that in our case plasticity is volume conserving, and that we need to consider only shear deformations. Hence in circular symmetry we have

$$D_{\theta\theta}^{\mathrm{pl}} = -D_{rr}^{\mathrm{pl}} \equiv D^{\mathrm{pl}}. \tag{2.18}$$

The constitutive behavior is introduced by writing D^{pl} as a function of the deviatoric stress s and the internal state fields. The material velocity at the edge of the hole $v(R,t)$ is just the rate of change of the hole radius

$$\dot{R}(t) = v(R,t) \tag{2.19}$$

and therefore, using the second equation in Eq. (2.9), we see that the hole evolves according to

$$\frac{\dot{R}}{R} = D_{\theta\theta}^{\mathrm{tot}}(R,t). \tag{2.20}$$

Once $D_{\theta\theta}^{\mathrm{tot}}(R,t)$ is specified, the last relation becomes an equation of motion for the boundary of the hole.

C. The velocity field

In order to explore the analytic structure of the problem, we use Eqs. (2.4), (2.9), (2.16), and (2.18) to obtain

$$\frac{v}{r} + \frac{\partial v}{\partial r} = -\frac{1}{K}\frac{\mathcal{D}p}{\mathcal{D}t} = -\frac{1}{K}\left[\dot{p} + v\frac{\partial p}{\partial r}\right], \tag{2.21}$$

$$\frac{v}{r} - \frac{\partial v}{\partial r} = \frac{1}{\mu}\frac{\mathcal{D}s}{\mathcal{D}t} + 2D^{\mathrm{pl}} = \frac{1}{\mu}\left[\dot{s} + v\frac{\partial s}{\partial r}\right] + 2D^{\mathrm{pl}}, \tag{2.22}$$

where overdots denote partial time derivatives. It is useful next to eliminate $\dot{s}(r,t)$ and $\dot{p}(r,t)$ from these equations, and thus to obtain a differential equation for the velocity field $v(r,t)$ that does not depend explicitly on those time derivatives. For that purpose, we operate with $-(\mu/Kr^2)(\partial/\partial r) \times [r^2(\cdots)]$ on Eq. (2.22), differentiate Eq. (2.21) with respect to r, add the results, and then use the partial time derivative of Eq. (2.14) to obtain

$$\left(1+\frac{\mu}{K}\right)\left(\frac{\partial^2 v}{\partial r^2} + \frac{1}{r}\frac{\partial v}{\partial r} - \frac{v}{r^2}\right) = -\frac{1}{K}\left[\frac{\partial v}{\partial r}\frac{\partial p}{\partial r} + v\frac{\partial^2 p}{\partial r^2} + \frac{1}{r^2}\frac{\partial}{\partial r}\left(r^2 v\frac{\partial s}{\partial r}\right)\right] - \frac{\mu}{K}\left(\frac{4D^{\mathrm{pl}}}{r} + 2\frac{\partial D^{\mathrm{pl}}}{\partial r}\right). \tag{2.23}$$

This is a linear second order differential equation for v with coefficients that are functions of $s(r,t)$ and $p(r,t)$. This equation can be further simplified by defining $\tilde{v} \equiv v/r$ and oper-

ating with $\partial_r[v(\cdots)]$ on Eq. (2.14). After simple manipulations we obtain

$$\left(1+\frac{\mu}{K}\right)\left(r\frac{\partial^2\tilde{v}}{\partial r^2}+3\frac{\partial\tilde{v}}{\partial r}\right)=\frac{2s}{K}\frac{\partial\tilde{v}}{\partial r}-\frac{\mu}{K}\left(\frac{4D^{\mathrm{pl}}}{r}+2\frac{\partial D^{\mathrm{pl}}}{\partial r}\right). \tag{2.24}$$

This equation requires two boundary conditions. To obtain these, we note that the first boundary condition of Eq. (2.15) implies

$$\frac{\mathcal{D}[p(R,t)+s(R,t)]}{\mathcal{D}t}=0. \tag{2.25}$$

Then, using Eqs. (2.21) and (2.22) and simple manipulations, we obtain

$$\frac{\partial\tilde{v}(R,t)}{\partial r}=-\frac{2K\tilde{v}(R)-2\mu D^{\mathrm{pl}}(R,t)}{(K+\mu)R}. \tag{2.26}$$

The last expression provides a relation between the boundary values, at $r=R$, of $\tilde{v}$ and $\partial_r\tilde{v}$. To provide Eq. (2.24) with enough boundary conditions, an additional boundary condition is required. It is convenient to obtain the boundary condition at infinity. To evaluate $\tilde{v}(\infty,t)$ we note that for $r\gg R$, the stress field is purely elastic and therefore the solution of Eq. (2.14) is $p=-\sigma^{\infty}$ and $s\sim r^{-2}$. Then, the large-r behavior of Eqs. (2.21) and (2.22) predicts that

$$\tilde{v}(\infty,t)=\frac{\dot{\sigma}^{\infty}}{2K}. \tag{2.27}$$

With this boundary condition at hand we can solve numerically Eq. (2.24) by adjusting $\tilde{v}(R,t)$ in Eq. (2.26) such that $\tilde{v}(\infty,t)$ satisfies Eq. (2.27).

In spite of the fact that we have a complete solution scheme, we supplement the derivation with an expression for $\tilde{v}(R)$ that will be proved useful later. To that aim we integrate Eq. (2.14) from $R(t)$ to ∞ and use the first boundary condition of Eq. (2.15) to obtain the integral relation

$$\sigma^{\infty}(t)=2\int_{R(t)}^{\infty}\frac{s(r,t)}{r}dr. \tag{2.28}$$

Taking the time derivative of Eq. (2.28), we obtain

$$\int_{R(t)}^{\infty}\frac{\dot{s}(r,t)}{r}dr=\frac{s(R,t)\dot{R}}{R}+\frac{\dot{\sigma}^{\infty}(t)}{2}. \tag{2.29}$$

In order to use the last result we operate with $\int_R^{\infty}(\cdots)(dr/r)$ on Eq. (2.22) to obtain

$$\tilde{v}(R)-\tilde{v}(\infty)=\frac{1}{\mu}\int_{R(t)}^{\infty}\frac{\dot{s}(r,t)}{r}dr+\frac{1}{\mu}\int_{R(t)}^{\infty}\tilde{v}(r,t)\frac{\partial s(r,t)}{\partial r}dr+2\int_{R(t)}^{\infty}\frac{D^{\mathrm{pl}}}{r}dr. \tag{2.30}$$

Substituting Eqs. (2.29) and (2.27) in Eq. (2.30) we find

$$\frac{\dot{R}}{R}=\tilde{v}(R,t)=\frac{2\int_R^{\infty}\frac{D^{\mathrm{pl}}(r,t)}{r}dr+\frac{1}{\mu}\int_{R(t)}^{\infty}\tilde{v}(r,t)\frac{\partial s(r,t)}{\partial r}dr+\dot{\sigma}^{\infty}(t)\left(\frac{1}{2\mu}+\frac{1}{2K}\right)}{1-\frac{s(R,t)}{\mu}}. \tag{2.31}$$

This equation plays a key role throughout the rest of this paper. As written here it provides an integral relation between $\tilde{v}(R,t)$ and $\tilde{v}(r,t)$ which can serve as a consistency check for our solution for Eq. (2.24). When the incompressible limit is taken, as seen below, this equation becomes an explicit expression for the velocity of the edge. Also note that it already incorporates the boundary conditions of Eq. (2.15).

D. Putting it all together

In order to put the equations in their final forms, up to specifying D^{pl}, we define

$$W(r,t)\equiv\frac{\partial\tilde{v}(r,t)}{\partial r}. \tag{2.32}$$

Then Eq. (2.24) becomes

$$\left(1+\frac{\mu}{K}\right)\left(r\frac{\partial W(r,t)}{\partial r}+3W(r,t)\right)=\frac{2s(r,t)}{K}W(r,t)-\frac{\mu}{K}\left(\frac{4D^{\mathrm{pl}}(r,t)}{r}+2\frac{\partial D^{\mathrm{pl}}(r,t)}{\partial r}\right), \tag{2.33}$$

which is to be solved using the boundary conditions given in Eqs. (2.26) and (2.27). The former becomes

$$W(R,t)=-\frac{2K\frac{\dot{R}}{R}-2\mu D^{\mathrm{pl}}(R,t)}{(K+\mu)R}. \tag{2.34}$$

In terms of $W(r,t)$, the equation of motion for the deviatoric stress $s(r,t)$, Eq. (2.22), is

$$-rW(r,t)=\frac{1}{\mu}\left[\dot{s}(r,t)+v(r,t)\frac{\partial s(r,t)}{\partial r}\right]+2D^{\mathrm{pl}}(r,t). \tag{2.35}$$

The pressure $p(r,t)$ can be calculated using Eq. (2.14). According to Eq. (2.32), the velocity field $v(r,t)$ is given by

$$v(r,t)=\frac{\dot{R}r}{R}+r\int_R^r W(r',t)dr'. \tag{2.36}$$

The initial conditions are the linear elastic fields determined by the load applied at $t=0$

$$p(r,t=0)=-\sigma^{\infty}(0),$$

$$s(r,t=0)=\sigma^{\infty}(0)\frac{R^2(0)}{r^2}. \tag{2.37}$$

III. PLASTIC DEFORMATION

To complete this theory, we need to choose a specific plastic rate-of-deformation function $D^{\mathrm{pl}}(s,\ldots)$ and equations of motion for the internal fields (denoted by the dots). As stated in the Introduction, we use the STZ theory described in Ref. [4]. Here, $D^{\mathrm{pl}}(s,\Lambda,m)$ depends on the deviatoric stress s, on the normalized STZ density Λ, and on a field m that describes the local average STZ orientation. Although ordinary thermal fluctuations are absent at the low temperatures considered here, the concept of an effective disorder temperature remains essential [4,5]. The effective temperature T_{eff} characterizes the state of configurational disorder in the system. It equilibrates to the ambient temperature T at high T (relative to the glass temperature T_g), but may fall out of equilibrium at low T where disorder is generated by the atomic-scale, configurational rearrangements that accompany mechanical deformations. We denote $T_{\mathrm{eff}}=(E_{\mathrm{STZ}}/k_B)\chi$, where E_{STZ} is a characteristic STZ formation energy; then the STZ density is proportional to the Boltzmann factor $\exp(-1/\chi)$. Most importantly, the time variation of the STZ density is slaved to the dynamics of χ.

The set of equations that describes plasticity in our theory [4] is

$$D^{\mathrm{pl}}(\tilde{s},m,\Lambda)=\frac{\epsilon_0}{\tau_0}\Lambda q(\tilde{s},m), \tag{3.1}$$

$$\frac{\mathcal{D}m}{\mathcal{D}t}=\frac{2}{\tau_0}q(\tilde{s},m)\left(1-\frac{m\tilde{s}}{\Lambda}e^{-1/\chi}\right), \tag{3.2}$$

$$\frac{\mathcal{D}\Lambda}{\mathcal{D}t}=\frac{2}{\tau_0}\tilde{s}q(\tilde{s},m)(e^{-1/\chi}-\Lambda), \tag{3.3}$$

$$\frac{\mathcal{D}\chi}{\mathcal{D}t}=\frac{2\epsilon_0}{c_0\tau_0}\Lambda\tilde{s}q(\tilde{s},m)(\chi_{\infty}-\chi), \tag{3.4}$$

where

$$q(\tilde{s},m)\equiv\mathcal{C}(\tilde{s})\left(\frac{\tilde{s}}{|\tilde{s}|}-m\right), \tag{3.5}$$

and $\tilde{s}=s/s_y$, with s_y being the dynamic yield stress [4]. Here τ_0 is an elementary time scale, ϵ_0 is a dimensionless constant of order unity, c_0 is a specific heat expressed in units of k_B per atom and thus is of order unity, and χ_{∞} is the asymptotic value approached by χ during continuous deformation [4].

Note that many of the features of these equations are model independent. For example, Eqs. (3.1) and (3.5) identify m as a "back stress" that governs an exchange of dynamic stability at $|\tilde{s}|=1$ (i.e., when $s=s_y$). For $|\tilde{s}|<1$, the stable steady-state solutions of these equations occur at $|m|=1$ such that the system is jammed and $D^{\mathrm{pl}}(\tilde{s},m,\Lambda)=0$. For $|\tilde{s}|>1$, on the other hand, $m=1/\tilde{s}$ and there is a nonvanishing plastic flow (see Ref. [4] for more details).

Essentially all of the specific material-dependent properties of this theory are contained in the function $\mathcal{C}(\tilde{s})$. In the STZ model described in Ref. [4], $\mathcal{C}(\tilde{s})$ is related to the rate $R(\tilde{s})$ at which STZ's transform between their two orientations:

$$\mathcal{C}(\tilde{s})\equiv\frac{\tau_0[R(\tilde{s})+R(-\tilde{s})]}{2}, \tag{3.6}$$

where $R(\tilde{s})$ is given by

$$R(\tilde{s})=\frac{2}{\tau_0}\int_0^{\tilde{s}}(\tilde{s}-\tilde{s}_{\alpha})P(\tilde{s}_{\alpha};\zeta)d\tilde{s}_{\alpha}, \tag{3.7}$$

$$P(\tilde{s}_{\alpha};\zeta)=\frac{\zeta^{\zeta+1}}{\zeta!}\tilde{s}_{\alpha}^{\zeta}e^{-\zeta\tilde{s}_{\alpha}}. \tag{3.8}$$

Here, $R(\tilde{s})$ is an integral over a distribution $P(\tilde{s}_{\alpha};\zeta)$ that reflects the fact that the STZ's can be of various types with different activation thresholds $\tilde{s}_{\alpha}$. The parameter ζ that characterizes the distribution is the only material parameter here; it controls the width of the distribution. The mean value of the distribution is s_y, the dynamic yield stress, that was shown in Ref. [4] to be the value of the deviatoric stress at which the system undergoes its dynamic exchange of stability from jammed to flowing states. For finite values of ζ there can be nonzero, sub-yield plastic deformation for $|\tilde{s}|<1$. This behavior is well documented in the literature [8]. We note that for $\tilde{s}$ very small or very large,

$$R(\tilde{s})\sim\tilde{s}^{\zeta+2}\quad\text{for }\tilde{s}\to 0^+, \tag{3.9}$$

$$R(\tilde{s})\simeq\tilde{s}-1\quad\text{for }\tilde{s}\gg 1. \tag{3.10}$$

A basic assumption of the STZ theory is that the STZ's are sparsely distributed and only weakly interacting with each other. For this assumption to be valid, χ_{∞} must be small. Indeed, in independent applications of the theory to actual materials [17] or simulations of such materials [5,18], χ_{∞} was found to be of order 0.15 or less. For such values of χ_{∞}, the density of STZ's, $\Lambda\cong\exp(-1/\chi_{\infty})$, is of order 10^{-3}, or very much smaller. We then notice that Λ appears as a rate-determining prefactor on the right-hand sides of Eqs. (3.1) and (3.4), which govern the bulk system-wide variables D^{pl}

and χ; but Λ does not appear in a similar way in Eqs. (3.2) and (3.3), which pertain to the dynamics of individual STZ's. It follows that the plastic strain rate and the effective temperature respond much more slowly to changes in stress than do the internal fields m and Λ, and that the slow dynamics of the effective temperature controls the observable mechanical behavior of the system in most circumstances. We conclude that, as long as the characteristic time scale of the external loading is not significantly smaller than $\tau_0 \exp(1/\chi_\infty)$, we can safely replace Eqs. (3.2) and (3.3) by their stationary solutions

$$m = m_0(\tilde{s}) = \begin{cases} \tilde{s}/|\tilde{s}| & \text{if } |\tilde{s}| \leqslant 1, \\ 1/\tilde{s} & \text{if } |\tilde{s}| > 1, \end{cases} \tag{3.11}$$

and

$$\Lambda = e^{-1/\chi}. \tag{3.12}$$

The approximation in Eq. (3.11) tells us that $|m|=1$ for all $|\tilde{s}|<1$, i.e., the system "immediately" becomes jammed at small stresses. In fact, one can think of an experiment in which at time $t=0$ a virgin material with $m=0$ throughout is being used. Then in regions where $\tilde{s}$ is small, m will remain very small for a long time, since $C(\tilde{s})$ is small. Notwithstanding, the precise value of m in regions of small $\tilde{s}$ is not important for any of the results presented below. Therefore, we use Eqs. (3.11) and (3.12) to reduce Eqs. (3.1)–(3.5) to

$$D^{\mathrm{pl}}(\tilde{s},m,\Lambda) = \frac{\epsilon_0}{\tau_0} e^{-1/\chi} q_0(\tilde{s}), \quad q_0(\tilde{s}) \equiv \mathcal{C}(\tilde{s}) \left(\frac{\tilde{s}}{|\tilde{s}|} - m_0(\tilde{s}) \right), \tag{3.13}$$

$$\frac{\mathcal{D}\chi}{\mathcal{D}t} = \frac{2\epsilon_0}{c_0 \tau_0} e^{-1/\chi} \tilde{s} q_0(\tilde{s})(\chi_\infty - \chi). \tag{3.14}$$

Once having made these simplifications, we also may go immediately to the limit $\zeta \to \infty$ and neglect any structure in the function $\mathcal{C}(\tilde{s})$ for stresses less than or of order of the yield stress. Without this approximation, our equations of motion would have predicted sub-yield deformations of magnitude proportional to $C(\tilde{s})\exp(-1/\chi_\infty)$, which we assume to be extremely small. Such deformations will not be negligible, of course, for soft and/or highly disordered systems, or for thermal systems at temperatures high enough to activate STZ transitions. But we do not need to consider such situations here, and therefore $\zeta \to \infty$ will suffice. In this limit, $\mathcal{C}(\tilde{s}) \approx \Theta(|\tilde{s}|-1)(|\tilde{s}|-1)$, where Θ is the Heaviside step function, and

$$q_0(\tilde{s}) \approx \Theta(|\tilde{s}|-1) \frac{(|\tilde{s}|-1)[\tilde{s}\,\mathrm{sgn}(\tilde{s})-1]}{\tilde{s}} \tag{3.15}$$

The initial conditions in Eqs. (2.37) must be supplemented with an initial condition for the effective temperature

$$\chi(r, t=0) = \chi_0, \tag{3.16}$$

where χ_0 describes a homogeneous state of disorder of the material before any load is applied. Because we are using Eq. (3.11), there is no comparable initial condition for m.

Equations (2.14), (2.21), (2.22), (2.31)–(2.36), and (3.13)–(3.15), and the initial conditions in Eqs. (2.37) and (3.16) define our problem. This system is specified by the following set of dimensionless parameters ϵ_0, c_0, χ_∞, χ_0, μ/s_y, K/s_y and a given loading scheme $\sigma^\infty(t)$. The first three parameters characterize our plasticity theory; χ_0 specifies the initial state of disorder of the material; and the last two parameters are the elastic moduli in units of the yield stress s_y. Note that two parameters τ_0 and s_y, are scaled out as units of time and stress, respectively. The only length scale in the problem is the initial radius of the hole which, without loss of generality, we set to unity.

IV. LOADING SCHEMES AND THE INCOMPRESSIBLE LIMIT

A. Loading schemes

We now specify the loading scheme $\sigma^\infty(t)$. To make contact with earlier work [9], we will look briefly in what follows at the case of increasing the load to a constant value, that is,

$$\sigma^\infty(t) = \begin{cases} \sigma_0 \dfrac{t}{500\tau_0}, & \text{for } 0 < t < 500\tau_0, \\ \sigma_0, & \text{for } t > 500\tau_0. \end{cases} \tag{4.1}$$

Our primary interest here, as in Ref. [9], will be to see how the region of plastic deformation forms, expands, and reaches a stable, stationary state for loading stresses σ_0 less than the threshold for unbounded growth of the hole (see the Appendix).

We will pay greater attention to a class of situations in which the load takes the form of a stress pulse of finite duration, because we believe that such a pulse may be relevant to fracture dynamics. Plastic deformation of a material failing by crack propagation is localized (if it happens at all) near the fracture surfaces. At any given material point, deformation occurs only during a short time interval as the crack tip passes nearby. Specifically, a material element lying ahead of a crack tip experiences first an increasing stress as the crack tip opens, and then a decreasing stress as the load vanishes on the newly formed—and deformed—fracture surfaces.

To simulate such a process in the circular geometry, we study a time-dependent loading scheme in which the remote stress $\sigma^\infty(t)$ increases monotonically from zero to a peak stress $\sigma_p > s_y$, and then returns monotonically to zero:

$$\sigma^\infty(t) = \begin{cases} 4\sigma_p \dfrac{t(T-t)}{T^2}, & 0 < t < T, \\ 0, & t > T. \end{cases} \tag{4.2}$$

An example with $T=8000\tau_0$ and $\sigma_p=2s_y$ is shown in Fig. 1.

Our choice of T in Eq. (4.2) is an order-of-magnitude estimate emerging from the analysis in Ref. [2]. For cracks whose speeds are governed by plastic dissipation, and when surface tension is negligible, that analysis implied that the crack tip blunts in such a way that the stress on its surface is always of order s_y, and the tip radius is linearly proportional

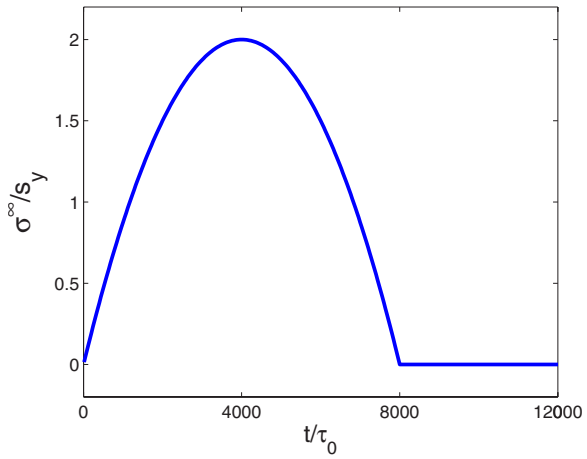

FIG. 1. (Color online) A time-dependent nonmonotonic loading scheme corresponding to Eq. (4.2) with $T=8000\tau_0$ and $\sigma_p=2s_y$.

to the crack speed. Thus the time T that any material element spends in the fracture zone is roughly constant, of order the plastic relaxation time $\tau_0 \exp(1/\chi_\infty)$. If $\chi_\infty \cong 0.13$, then $T \cong 2200\tau_0$. This estimate is consistent with the discussion in Ref. [3], where the plastic zone size was dynamically adjusted so that the time needed for the crack to pass this zone was of the order of the plastic relaxation time. Note that T is a very short time, of order picoseconds if τ_0 is an atomic time of order femtoseconds. That value of T is roughly an atomic spacing divided by a sound speed. These estimates lead us to believe that, although STZ plasticity is slow on atomic time scales, it is easily fast enough to be relevant to fracture. Clearly, this estimate of relevant time scales will have to be reexamined when the theory is applied to realistic models of fracture where surface tension is important.

B. The incompressible limit

It is convenient for both analytic and numerical simplicity to work in the limit of elastic (as well as plastic) incompressibility. Many materials are highly incompressible, as evidenced by large bulk moduli K or, equivalently, by the two-dimensional Poisson ratios ν^* being close to unity. Moreover, we have studied numerically the set of equations (2.14), (2.21), (2.22), (2.32)–(2.37) and (3.1)–(3.8) for various loading scenarios using $0.7 \leqslant \nu^* < 1$, and have found results that vary smoothly with ν^* without any noticeable singular behavior in the limit $\nu^* \to 1$. Therefore, for analytic purposes, we can focus on the limit $\nu^* \to 1$ $(K \to \infty)$.

Note first that, in the incompressible limit, Eq. (2.21) reduces to

$$\frac{v}{r} + \frac{\partial v}{\partial r} = 0, \tag{4.3}$$

which is in accord with the zero total compressibility $\mathrm{tr}\boldsymbol{D}^{\mathrm{tot}} = 0$. Equation (4.3) can immediately be integrated to yield

$$v(r,t) = \frac{\dot{R}(t)R(t)}{r}, \tag{4.4}$$

where the boundary condition (2.19) has been used. This explicit expression for the velocity field provides a major simplification because we no longer need to solve Eq. (2.33)–(2.36) numerically.

Having the velocity field at hand, we can rewrite all the equations of the theory in a more explicit way. The sum of Eqs. (2.21) and (2.22) becomes

$$\frac{\dot{R}R}{r^2} = \frac{1}{2\mu}\frac{\partial s}{\partial t} + \frac{1}{2\mu}\frac{\dot{R}R}{r}\frac{\partial s}{\partial r} + D^{\mathrm{pl}}. \tag{4.5}$$

Equations (3.13)–(3.15) (with $\tilde{s}=s/s_y$ as before) are

$$D^{\mathrm{pl}} = \frac{\epsilon_0}{\tau_0} e^{-1/\chi} q_0(\tilde{s}), \quad q_0(\tilde{s}) = \Theta(|\tilde{s}|-1)\frac{(|\tilde{s}|-1)[\tilde{s}\,\mathrm{sgn}(\tilde{s})-1]}{\tilde{s}}; \tag{4.6}$$

$$\frac{\partial \chi}{\partial t} + \frac{\dot{R}R}{r}\frac{\partial \chi}{\partial r} = \frac{2}{c_0}\frac{\varepsilon_0}{\tau_0} e^{-1/\chi}\tilde{s} q_0(\tilde{s})(\chi_\infty - \chi). \tag{4.7}$$

The derived relation (2.31) becomes

$$\frac{\dot{R}}{R} = \frac{2\int_R^\infty \frac{D^{\mathrm{pl}}}{r}dr + \frac{\dot{\sigma}^\infty(t)}{2\mu}}{1 - \frac{2R^2}{\mu}\int_R^\infty \frac{s(r,t)}{r^3}dr}. \tag{4.8}$$

Note that the pressure $p(r,t)$ does not appear in the final equations for the incompressible limit, but is computable as before from the deviatoric stress field $s(r,t)$ using Eq. (2.14).

V. RESULTS

We are now ready to study numerically Eqs. (4.5)–(4.8) in detail. We consider both the constant load and the time-dependent loading scenarios, Eqs. (4.1) and (4.2), respectively.

A. Increase toward a constant load

The results of numerical simulations for the case of an increase toward a constant load $\sigma_0/s_y=2$ are shown in Fig. 2. In this loading scheme, we know that there is a maximum value of σ^∞, say σ^{th}, above which the hole expands indefinitely. (See Ref. [9] and earlier references cited there.) For completeness, in the Appendix, we show how to compute σ^{th} in the current version of STZ theory. The result, for the parameters used here, is $\sigma^{\mathrm{th}} \approx 5s_y$, which is substantially larger than the value of σ_0 chosen for this illustration.

Note that the radius of the hole, $R(t)$, first increases elastically to $R_0=\exp(\sigma_0/2\mu) \cong 1.02$ (not shown in Fig. 2), then grows (by less than one percent in this example), and tends toward a constant value at large times. The stress s is proportional to the elastic solution $1/r^2$ for r outside the plastically deformed region; but, in accordance with conventional

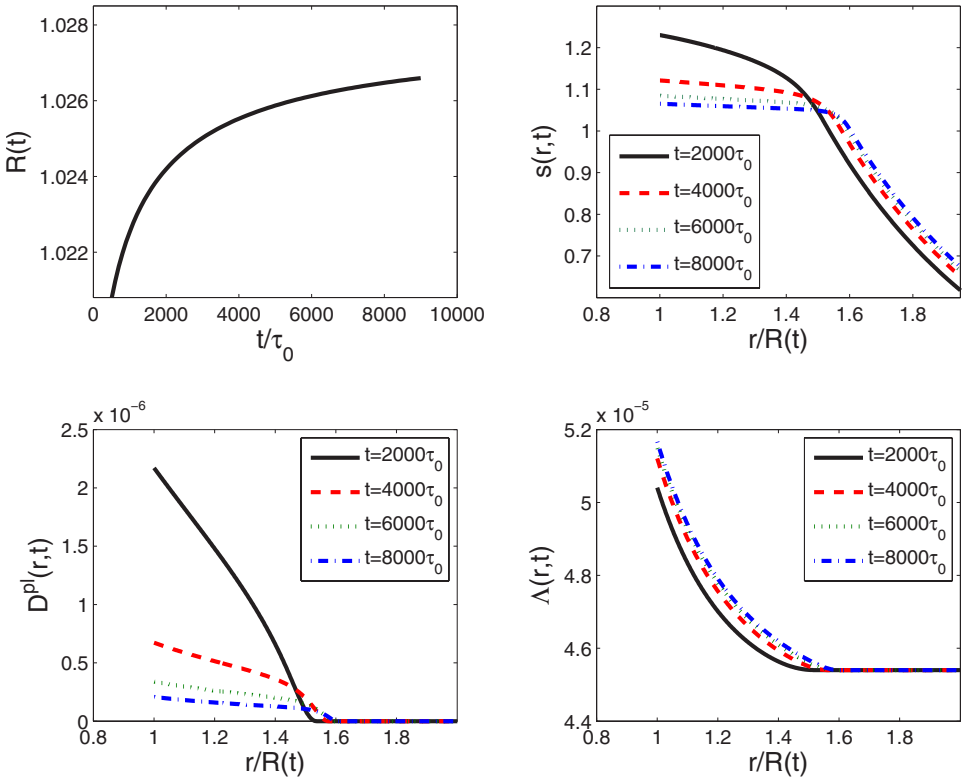

FIG. 2. (Color online) The r dependence of the dynamical variables at different times in the constant load case. The radius of the circle is shown in the upper left panel without the initial elastic expansion. At longer times the radius saturates. Note the relative small increase in radius. The stress is shown in the upper right panel, and the fields $D^{\mathrm{pl}}(r,t)$ and $\Lambda=e^{-1/\chi}$ in the two lower panels, respectively. The parameters chosen are $\epsilon_0=1$, $c_0=1$, $\chi_0=0.13$, $\chi_0=0.1$, $\mu=50s_y$, and $\sigma_0=2s_y$. The solid line corresponds to $t=2000\tau_0$, the dashed line to $t=4000\tau_0$, the dotted line to $t=6000\tau_0$, and the dotted-dashed line to $t=8000\tau_0$.

plasticity theories, s decreases in time toward the yield stress s_y inside that region. The plastic region eventually extends out to a radius R_1. The usual quasistatic estimate of R_1 [8,9] is made by assuming $s(r)=s_y$ for $R<r<R_1$, and $s(r)=s_y(R_1/r)^2$ for $r>R_1$. Inserting this $s(r)$ into the integral on the right-hand side of Eq. (2.28) and setting $\sigma^\infty=\sigma_0=2s_y$ on the left-hand side, we find $R_1/R=\exp[(1/2)(\sigma_0/s_y-1)]=1.65$. Thus, even in cases where the plastic deformation is small in comparison to the elastic displacement, the plastically deformed region may be quite extensive. Finally, note that the STZ density $\Lambda=e^{-1/\chi}$ becomes substantially larger than its initial value throughout this plastic region.

B. Time-dependent nonmonotonic loading

In Figs. 3 and 4 we present numerical results for the case of time-dependent nonmonotonic loading as shown in Eq. (4.2) and Fig. 1. Here we have chosen $T=8000\tau_0$ and two different values of the peak stress $\sigma_p/s_y=2.0$ and 4.0. The first of these is small enough that the radius of the hole changes at its maximum by only about two percent, consistent with the effect of constant loading at the same stress shown in Fig. 2. Only a small part of that transient change in the radius is irreversible plastic deformation; most of what we are seeing is elastic expansion and contraction of the system as a whole. However, this relatively moderate scenario may be the more realistic of the two sets of time-dependent simulations for describing failure in strong structural materials where, in keeping with conventional analyses, we do not expect stresses to be much larger than the yield stress.

The bigger peak stress causes substantially more plastic deformation, as seen in the comparatively large, irreversible change in the hole radius that remains after the system has been fully unloaded. This peak stress may be unrealistically large; but showing it here illustrates some features of the plastic response more clearly than the small-stress case. Note that the large applied stress induces a complex unloading sequence in which the stress near the hole becomes so large and negative that it drives strain recovery via reverse plastic deformation.

The dynamic response of this system, in both examples, is characterized by the emergence of a residual stress in the plastic zone near the hole edge. Note that s exhibits the sharp transition between plastic and elastic regions that we expect as a result of the special form of the constitutive law chosen in Eq. (3.15), and that the STZ density Λ becomes large in the plastic region. The qualitative picture that we take from these results is that of a plastically deformed region near the hole edge (or near any defect boundary in the general case), outside of which s retains its elastic solution (here proportional to $1/r^2$), but within which s decreases and may change sign, consistent with an irreversible outward displacement of the material near the hole.

VI. BOUNDARY-LAYER APPROXIMATION

A principal objective of this investigation has been to study the dynamics of time-dependent plasticity in the neighborhood of a symmetrically loaded circular hole and, from this study, to learn how to construct realistic approximations for less symmetric situations. We have seen in the preceding section that, under certain circumstances, plastic deformation remains localized in a relatively narrow zone near the hole. This observation leads us to believe that some sort of

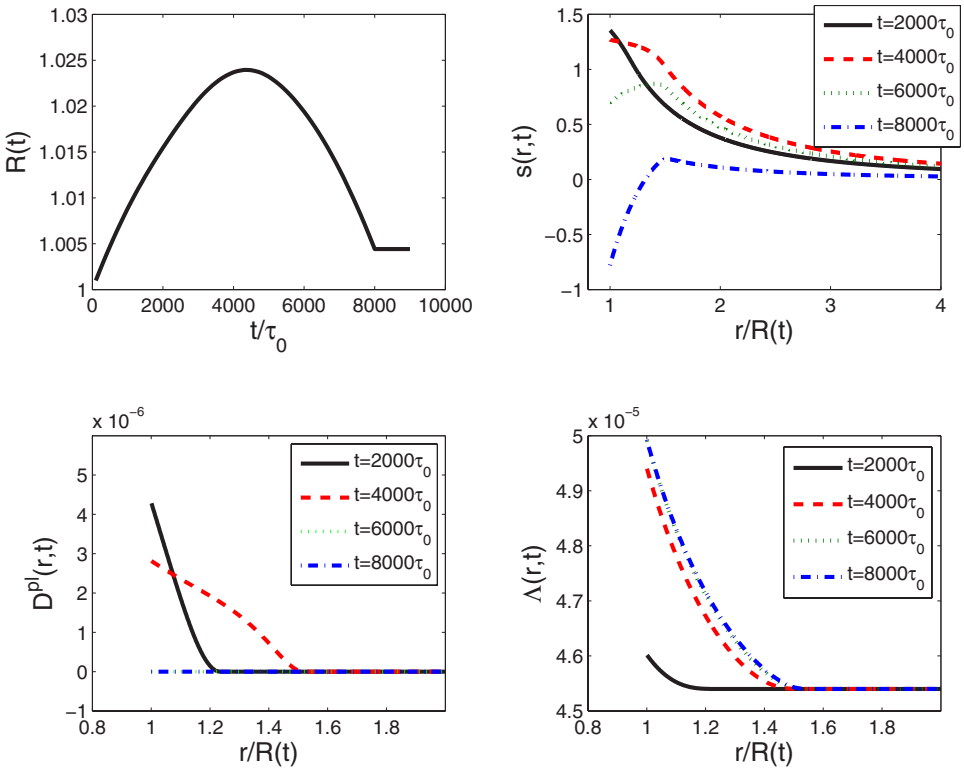

FIG. 3. (Color online) The time-dependent nonmonotonic load case. All the material parameters are the same as those for Fig. 2, while the load is given by Eq. (4.2) with $T=8000\tau_0$ and $\sigma_p=2s_y$. The solid line corresponds to $t=2000\tau_0$, the dashed line to $t=4000\tau_0$, the dotted line to $t=6000\tau_0$, and the dotted-dashed line to $t=8000\tau_0$.

boundary-layer approximation might have at least limited validity in interesting applications such as asymmetric void growth or fracture. In what follows, we explore one class of such approximations.

The numerical examples illustrated in Figs. 3 and 4 have several common features that need to be captured in any useful approximation. Most importantly, the dynamic behavior is qualitatively different in what we call the "active plastic phase"—roughly speaking, the time interval in which the hole is growing by plastic deformation—than it is in the "elastic unloading phase" where plastic deformation ceases. During the active plastic phase, as soon as σ^∞ exceeds s_y, plastic deformation occurs in an active plastic zone $R(t)<r<R_1(t)$, where $R_1(t)$ is the radius at which

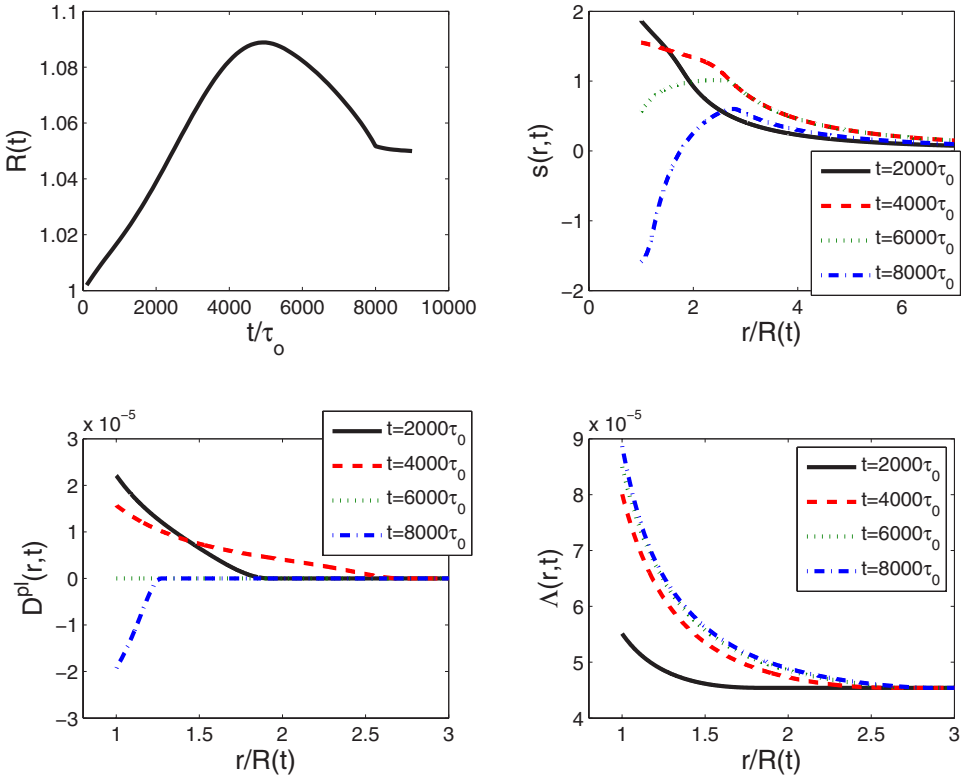

FIG. 4. (Color online) Same as the preceding figure but with $\sigma_p=4s_y$.

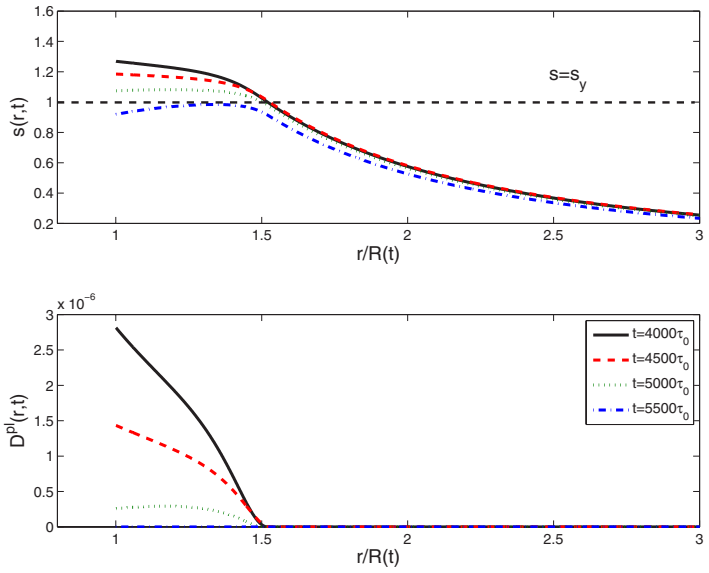

FIG. 5. (Color online) The profiles of $s(r,t)$ and $D^{\mathrm{pl}}(r,t)$ for the same external loading as in Fig. 3. The solid line corresponds to $t=4000\tau_0$, the dashed line to $t=4500\tau_0$, the dotted line to $t=5000\tau_0$, and the dotted-dashed line to $t=5500\tau_0$.

$$s[R_1(t),t] = s_y. \tag{6.1}$$

During this phase, no irreversible deformation has occurred for $r>R_1(t)$, and thus the stress field in this outer region is simply

$$s(r,t) = s_y \frac{R_1^2(t)}{r^2}, \quad p(r,t) = -\sigma^{\infty}(t), \quad \text{for } r > R_1. \tag{6.2}$$

This behavior changes as elastic unloading begins. As seen in Figs. 3 and 4, $R(t)$ reaches its peak considerably later than when the load $\sigma^{\infty}(t)$ peaks at $t_p=4000\tau_0$. Between t_p and the time at which $R(t)$ reaches its maximum, and for some time after that, the hole continues to grow plastically while the system as a whole contracts elastically. During that interval, the stress at the boundary of the hole, $s(R,t)$, drops rapidly toward the yield stress s_y; while $s(R_1,t)$, by the definition of R_1, remains equal to s_y. The transition between the active plastic and the elastic unloading phases that is important for our purposes occurs when $s(R,t)$ passes downward through s_y at a time that we call t_1.

To see what happens near t_1, we show in Fig. 5, for the case $\sigma_p=2s_y$, a sequence of graphs of $s(r,t)$ and $D^{\mathrm{pl}}(r,t)$ as functions of $r/R(t)$ for four equally spaced times starting at $t_p=4000\tau_0$, and ending at $t=5500\tau_0$ (just later than $t_1 \cong 5200\tau_0$). Note that at $t=5500\tau_0$ D^{pl} has already vanished. The crucial observation is that $D^{\mathrm{pl}}(r,t)$ extends across the whole active plastic zone, $R(t)<r<R_1(t)$, until $t=t_1$, at which time, at least to a rough first approximation, it vanishes almost uniformly everywhere.

The elastic unloading phase, starting at about time t_1, evolves as an entirely elastic response to the decreasing driving force, conditioned by the material displacements that occurred during the plastic loading phase. During this part of the unloading process, there is no longer an active plastic zone, but there remains a plastically deformed region—a "process zone"—within which irreversible material displacements give rise to residual stresses. The process zone extends from $R(t)$ out to the most distant material point at which plastic deformation occurred, that is, out to $R_1(t_1)$ advected back toward $R(t)$ by elastic relaxation.

Elastic unloading persists at least until $t=T$ when the remote load $\sigma^{\infty}(t)$ vanishes. As seen in Fig. 4, the stress near the hole may become so large and negative that it drives plastic strain recovery. This behavior occurs only for large peak stresses, and does not occur when the remote stresses are smaller than about $2.5s_y$ in the present model. We will not include plastic strain recovery in our boundary-layer analysis, and simply will point out where it is missing.

Our strategy for developing a boundary-layer approximation is to write equations of motion for quantities defined only near the boundary, i.e., within the process zone, and then to deduce the boundary motion from these local quantities instead of solving for fields everywhere in the system. In our case, the relevant boundary is just the hole radius $R(t)$. The rate of change of any quantity $A(R,t)$, defined on $r=R(t)$, is

$$\frac{dA(R,t)}{dt} = \frac{\partial A(R,t)}{\partial t} + \dot{R}\frac{\partial A(R,t)}{\partial r}. \tag{6.3}$$

Since $\dot{R}=v(R,t)$, the time derivative in Eq. (6.3) is just the material time derivative defined in Eq. (2.11). The equations for $s(R,t)$, $D^{\mathrm{pl}}(R,t)$ and $\chi(R,t)$, i.e., Eqs. (4.5)–(4.7) evaluated at $r=R(t)$, are

$$\frac{\dot{R}}{R} = \frac{1}{2\mu}\frac{ds(R,t)}{dt} + D^{\mathrm{pl}}(R,t), \tag{6.4}$$

$$D^{\mathrm{pl}}(R,t) = \frac{\epsilon_0}{\tau_0} e^{-1/\chi(R,t)} q_0(R,t), \quad q_0(R,t) \equiv q_0[\bar{s}(R,t)], \tag{6.5}$$

$$\frac{d\chi(R,t)}{dt} = \frac{2\epsilon_0}{c_0\tau_0} e^{-1/\chi(R,t)} s(R,t) q_0(R,t)[\chi_\infty - \chi(R,t)]. \tag{6.6}$$

We need one more relation to close this set of equations. The obvious candidate is Eq. (4.8), which already involves only quantities defined in the process zone. This equation demands special attention, however, because it has been derived using exact mathematical relationships that are unique to circular symmetry, and because it explicitly involves the remote driving force $\sigma^\infty(t)$ which entered the analysis *via* those exact relationships. We need some such relation to determine the coupling between the remote driving force and the boundary. If the boundary-layer strategy is to be successful, we ultimately will have to interpret $\sigma^\infty(t)$ as a quantity emerging from solutions of a more general elasticity problem. For present purposes, however, we accept Eq. (4.8) as written, except that we simplify it by neglecting the integral term in the denominator since $s(R,t)/\mu$ is at most of the order of s_y/μ which is itself much smaller than unity. Thus we write

$$\frac{\dot{R}}{R} \cong 2\int_R^{R_1} \frac{D^{\mathrm{pl}}(r,t)}{r} dr + \frac{\dot{\sigma}^\infty(t)}{2\mu}. \tag{6.7}$$

Note that the original integral in Eq. (4.8) involves the plastic rate of deformation $D^{\mathrm{pl}}(r,t)$ which vanishes for $r > R_1$. Therefore, in Eq. (6.7), we have explicitly inserted R_1 as the upper limit of integration.

Next we use Eq. (6.7) to obtain an approximate expression for $\dot{R}/R$, and then use that relation to eliminate $\dot{R}/R$ on the left-hand side of Eq. (6.4) in favor of $s(R,t)$. To do this, we need an approximation for the integral over $D^{\mathrm{pl}}(r,t)$ that appears in Eq. (6.7). The numerical results shown in Fig. 5 suggest that, throughout the active plastic phase, $D^{\mathrm{pl}}(r,t)$ varies almost linearly, from its value $D^{\mathrm{pl}}(R,t)$ at $r=R(t)$ to zero (by definition) at $r=R_1(t)$. Thus we write

$$\int_R^{R_1} \frac{D^{\mathrm{pl}}(r,t)}{r} dr \cong \frac{1}{2} D^{\mathrm{pl}}(R,t)\left(\frac{R_1(t)}{R(t)} - 1\right). \tag{6.8}$$

To estimate $R_1(t)$ we invoke Eq. (2.28), which is another exact relationship between the circularly symmetric stress field $s(r,t)$ and the remote driving force $\sigma^\infty(t)$, and is subject to the same concerns that we expressed above about our use of Eq. (4.8). So long as we remain in the active plastic phase, and can assume that $R_1(t)$ remains the outer boundary of the material region in which $D^{\mathrm{pl}}(r,t)$ is nonzero, we can use Eq. (6.2) for the stress outside $r=R_1(t)$, and write Eq. (2.28) in the form

$$\sigma^\infty(t) = 2\int_{R(t)}^{R_1(t)} \frac{s(r,t)}{r} dr + s_y. \tag{6.9}$$

Then, in the spirit of our approximation for $D^{\mathrm{pl}}(r,t)$ in the active plastic region, we make a linear approximation for $s(r,t)$, using the fact that this stress is equal to s_y at R_1, and allowing $s(R,t) \equiv s[R(t),t]$ to be an as yet undetermined function of time. Specifically, for $R(t) < r < R_1(t)$ and for times $t < t_1$ such that $s(R,t) \geqslant s_y$, we have

$$s(r,t) \cong s_y + \frac{R_1(t) - r}{R_1(t) - R(t)}[s(R,t) - s_y], \quad s(R,t) > s_y. \tag{6.10}$$

Inserting Eq. (6.10) into Eq. (6.9), and linearizing in $(R_1 - R)/R$, we find, again for $t < t_1$,

$$\left(\frac{R_1(t)}{R(t)} - 1\right) \cong \frac{\sigma^\infty(t) - s_y}{s(R,t) + s_y}, \quad \sigma^\infty(t), s(R,t) > s_y. \tag{6.11}$$

Note that when $\sigma^\infty(t)$ is increasing and is smaller than s_y, there is no active plastic zone at all, i.e., $R_1(t) = R(t)$. Using Eq. (6.8) and (6.11), Eq. (6.7) becomes

$$\frac{\dot{R}}{R} \cong \frac{\sigma^\infty(t) - s_y}{s(R,t) + s_y} D^{\mathrm{pl}}(R,t) + \frac{\dot{\sigma}^\infty(t)}{2\mu}, \quad \sigma^\infty(t), s(R,t) > s_y. \tag{6.12}$$

We emphasize that, in this approximation, the end of the active plastic phase occurs at the time t_1 when $s(R,t_1) = s_y$. By definition, $D^{\mathrm{pl}}(R,t_1) = 0$, and therefore $D^{\mathrm{pl}}(r,t_1) \cong 0$ throughout $R(t_1) < r < R_1(t_1)$. Apart from the possibility of reverse plasticity, $D^{\mathrm{pl}}(r,t)$ vanishes at all later times, $t > t_1$. It follows that Eq. (6.12), with a properly interpreted $D^{\mathrm{pl}}(r,t)$, is a valid approximation at all times, during loading and unloading, because—apart from the possibility of reverse plasticity—$D^{\mathrm{pl}}(R,t)$ vanishes whenever $s(R,t) < s_y$.

Our boundary-layer calculation is straightforward from here on. We insert Eq. (6.12) on the left-hand side of Eq. (6.4), thus obtaining a nonlinear, first-order differential equation for $s(R,t)$, which can be solved using Eqs. (6.5) and (6.6). Our results are shown in Figs. 6–8, where we compare the predictions of the boundary layer theory for $R(t)$, $s(R,t)$, $D^{\mathrm{pl}}(R,t)$, and $\Lambda(R,t)$ with the exact solutions for $\sigma_p/s_y = 2$, 3, and 4. The comparison is excellent for $\sigma_p/s_y = 2$, even though $R_1(t)/R(t) - 1$ is about 0.5, which is not that small. The results are acceptable also for $\sigma_p/s_y = 3$, but deviations grow rapidly for higher values of σ_p/s_y, as expected. Note that in Figs. 7 and 8 the effect of plastic strain recovery is noticeable for the exact solution but has not been included in the boundary-layer approximation. Nevertheless, the values $s[R(t)] < -s_y$ and $D^{\mathrm{pl}}[R(t)] < 0$ are well approximated in this period of plastic strain recovery.

We can push the comparison between the boundary-layer approximation and the exact results further by computing the residual stresses in the process zone. We do this as follows. We note first that Eq. (6.4) can be used for any radius $R'(t)$, not just the radius of the hole $R(t)$. At times later than t_1, the quantity $D^{\mathrm{pl}}(R',t)$ appearing here vanishes for any R'. We also can compute the quantity $\dot{R}'/R'$ on the left-hand side of Eq. (6.4) using our knowledge of $\dot{R}(t)/R(t)$ and the fact that the material in the region between R and R' is incompressible $(R'\dot{R}' = R\dot{R})$. Finally, we know that $s(R',t_1) \cong s_y$ for all R' between R and R_1; so we can use Eq. (6.4) to compute the

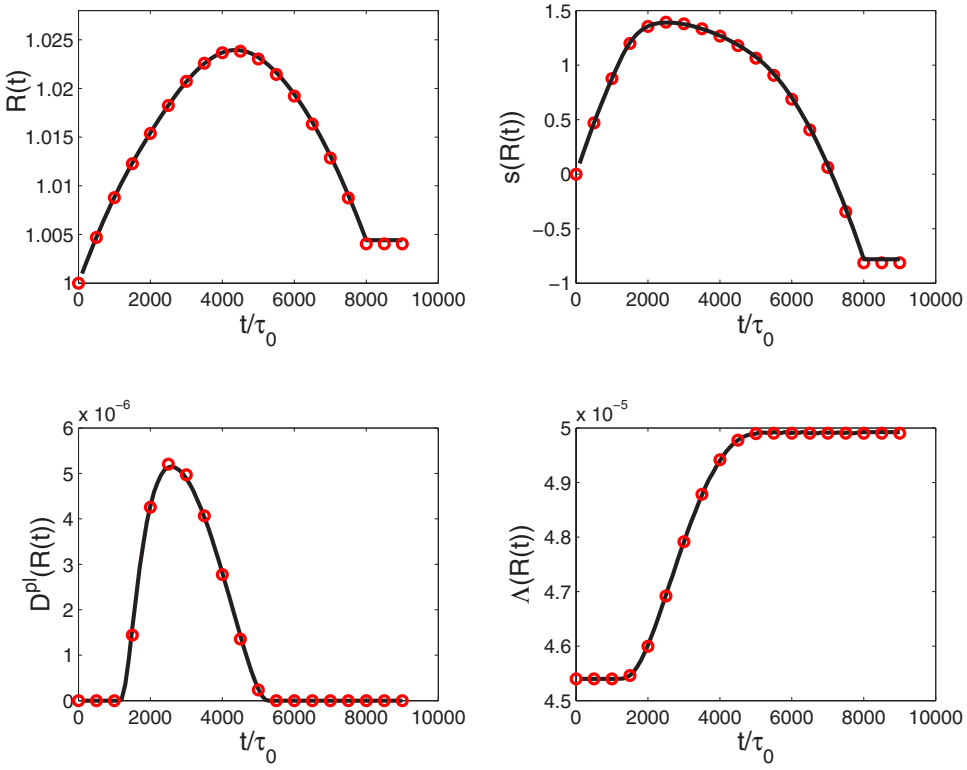

FIG. 6. (Color online) A comparison between the exact solution (solid line) and the prediction of the boundary layer theory (open circles) for $\sigma_p = 2s_y$.

advected value of $s[R'(t),t]$ at any later time t, and then plot this value as a function of the advected position $r=R'(t)$. The functions $s(r,t)$ computed in this way, for $\sigma_p/s_y=2$, are shown in Fig. 9. Outside the process zone, we have used the elastic solution with $s \propto 1/r^2$. The agreement between the full solution and the boundary layer predictions lends further support to the philosophy presented in this section.

VII. DISCUSSION AND SUMMARY

We have presented a derivation of the equations of motion for a moving free boundary, in this case a circle, using the athermal STZ theory of amorphous plasticity. To afford some analytic steps we have made several simplifying approximations. These are (i) inertia in the equations of motion was neglected. This approximation will be removed in a

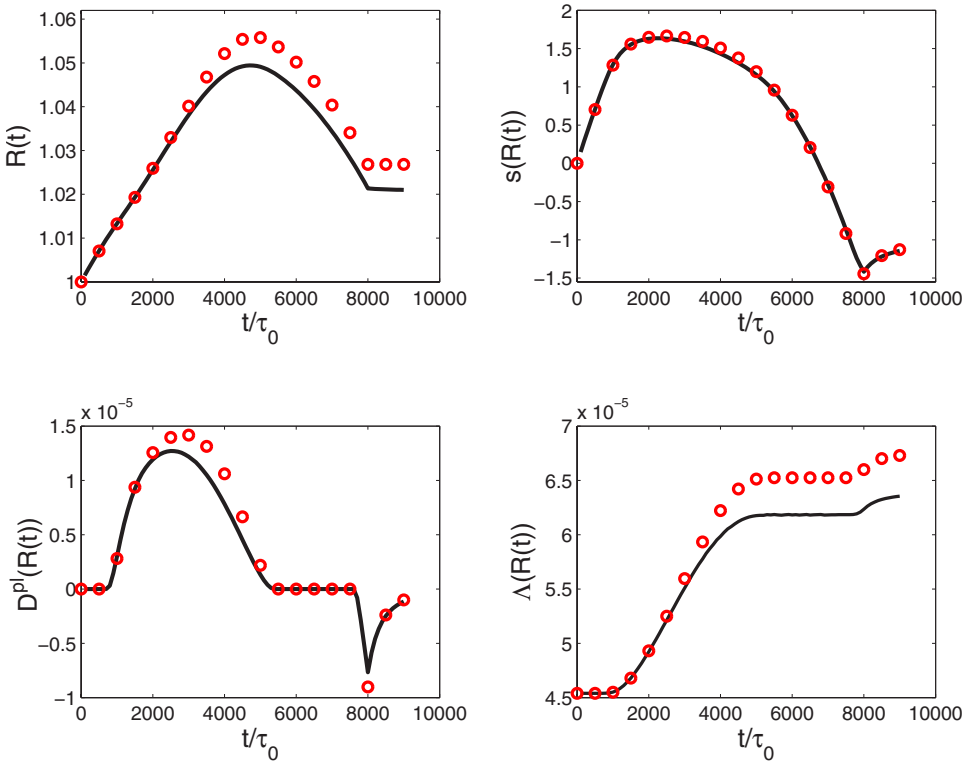

FIG. 7. (Color online) A comparison between the exact solution (solid line) and the prediction of the boundary layer theory (open circles) for $\sigma_p = 3s_y$.

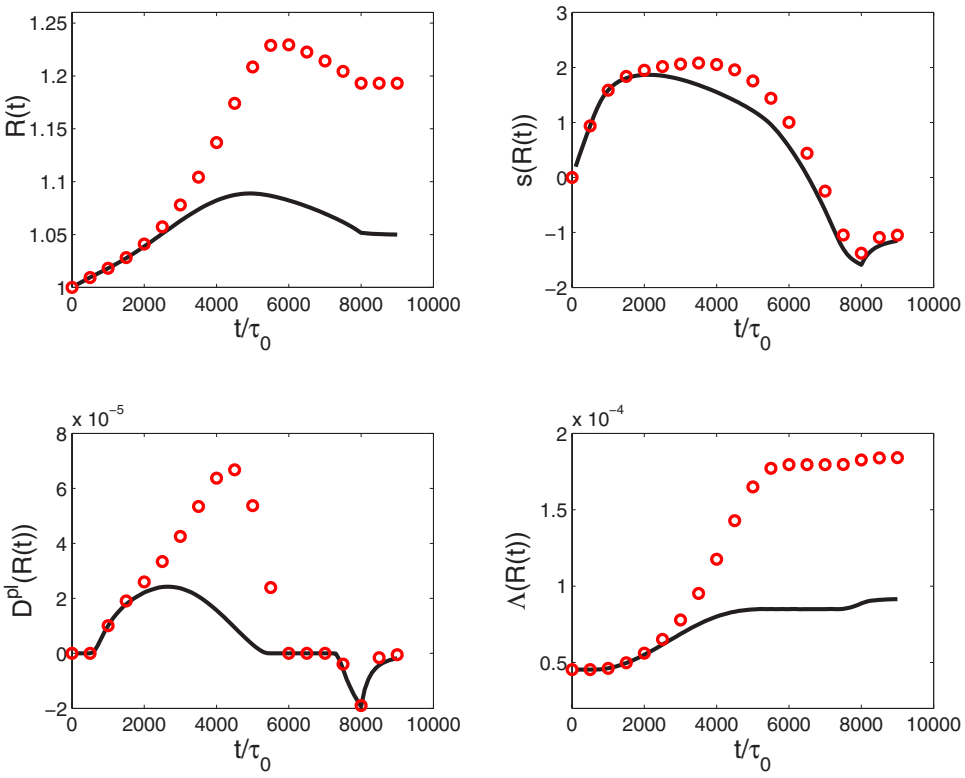

FIG. 8. (Color online) A comparison between the exact solution (solid line) and the prediction of the boundary layer theory (open circles) for $\sigma_p = 4s_y$.

follow-up paper. (ii) The incompressible limit was shown to be regular and useful for analytic progress. (iii) Small elastic deformations were assumed, allowing us to employ the additive decomposition of the total rate of deformation tensor, and linear elasticity. (iv) In the STZ theory we used the separation of time scales between the dynamics of m and χ to slave the fast to the slow variables using the fixed points of m. Finally, we simplified the function $C(\tilde{s})$ by neglecting the sub-yield deformations. The resulting equations were solved numerically and yielded some interesting results. We looked especially at loading scenarios in which the material was subjected, at large distances from the hole, to stress pulses

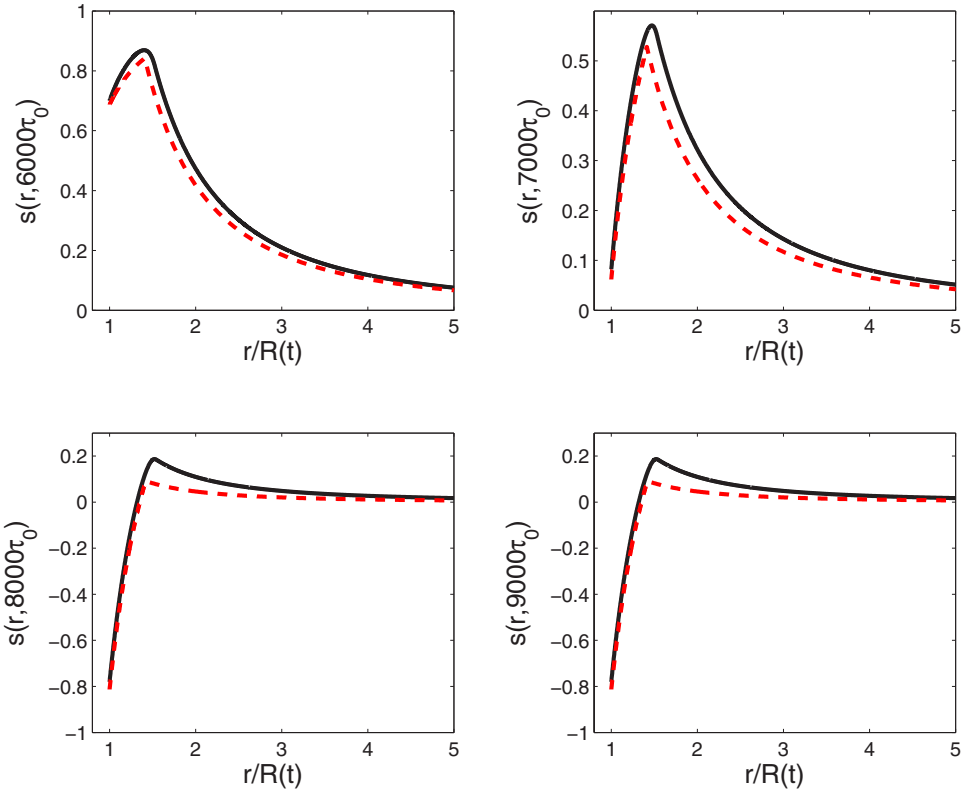

FIG. 9. (Color online) Comparison between the full solution (solid line) for $s(r,t)$ and the prediction of the boundary layer approximation (dashed line) for $\sigma_p = 2s_y$ and for various values of t.

whose durations were comparable to the plastic relaxation time for the STZ mechanism. For the range of material parameters chosen here, which we believe to be characteristic of realistic amorphous solids, the irreversible displacement of the boundary of the hole was small. However, the width of the region in which plastic deformation occurred, as evidenced by increased internal disorder and residual stresses, became comparable to the radius of the circle for stress pulses whose peak strengths σ_p were twice the yield stress s_y. We also found that strong enough stress pulses $\sigma_p \geqslant 2.5 s_y$ induce reverse, plastic strain recovery near the edge of the hole.

The theory as written is rather cumbersome even for the circular symmetry considered here. It is therefore with some relief that we have found that a boundary layer approximation, using only quantities defined on the circumference of the circle and their coupling to the remote stress, succeeds in capturing the plastic effects quite well. Specifically, despite several apparently serious oversimplifications, this approximation accurately reproduces the irreversible displacement of the radius of the circle and the residual stress found in its neighborhood. We propose that such boundary layer theories might find useful applications in less symmetric situations, not the least interesting being fracture dynamics.

A next issue on our agenda is the dynamic stability of our circular solutions. It will be interesting to learn whether our equations of motion predict that the growing circular hole becomes unstable against symmetry-breaking perturbations, for example, whether it forms fingers that might evolve into cracks, or whether a perturbed circular solution can survive. The transition between these two possibilities, if found, might shed light on the brittle-to-ductile transition in viscoplastic materials. Along the same lines, it will be important to learn how strongly the circular behavior itself, and the stability of circular symmetry, depend on specific details of our model such as elastic compressibility, initial states of disorder, or the absence of thermal effects.

ACKNOWLEDGMENTS

We thank A. Lemaitre for illuminating discussions and E. Shtilerman for carefully reading the manuscript. This work was supported in part by the Minerva Foundation with funding from the Federal German Ministry for Education and Research, the Israel Science Foundation and the German Israeli Foundation. E.B. was supported by the Horowitz Complexity Center. J.S.L. was supported by U.S. Department of Energy Grant No. DE-FG03-99ER45762. T.S.L. was supported in part by the European Commission via a TMR grant.

APPENDIX: UNBOUNDED GROWTH

One characteristic stress that emerges in the circular-hole problem is the threshold σ^{th} above which the hole grows without bound under conditions of constant loading. In this section we explain how this threshold is estimated in the athermal STZ theory.

Because the only length scale in this problem is the radius of the hole $R(t)$, we expect that all spatially varying (r-dependent) quantities occurring in a uniformly (exponentially) expanding solution of our equations of motion will be self-similar functions only of the ratio $r/R(t)$. For convenience, we choose the variable $\xi = R(t)/r$. These self-similar solutions are characterized by $\dot{R}/R = \omega$, where $\omega > 0$ depends on the loading and vanishes at the threshold σ^{th}.

In fact, these solutions invalidate the assumptions of our theory for large times since the exponential growth of the hole implied by $\dot{R}/R = \omega$ will inevitably lead to very large velocities at large t, in contradiction with our omission of the inertial term in Eq. (2.7). When this happens in the full, inertial theory, the self-similar solutions break down with the appearance of perturbations propagating at a characteristic wave velocity. Nevertheless, as we are interested in obtaining an estimate for σ^{th}, the self-similar approximate solutions for finite times are still useful. .

For present purposes, we solve our equations of motion for a self-similar deviatoric stress $\tilde{s}(\xi;\omega)$ in the limit $\tau_0\omega \to 0$. Once $\tilde{s}(\xi;\omega)$ is known, we can use Eq. (2.28) to obtain the following expression for σ^{th}:

$$\frac{\sigma^{\text{th}}}{s_y} \simeq 2\int_0^1 \frac{\tilde{s}(\xi;\omega)}{\xi} d\xi \quad \text{for } \tau_0\omega \to 0. \tag{A1}$$

Here we assume that the exponential growth at a small ω allows the system to approach the self-similar solution $\tilde{s}(\xi;\omega)$ in times when the velocities are still smaller than the typical wave velocity. $\tilde{s}(\xi;\omega)$ can be computed using Eqs. (4.5)–(4.7). First we note that the material time derivative of Eq. (2.11) translates to

$$\frac{\mathcal{D}}{\mathcal{D}t} = \omega\xi(1-\xi^2)\frac{\partial}{\partial\xi}. \tag{A2}$$

Then Eqs. (4.5)–(4.7) read

$$\tau_0\omega\xi(1-\xi^2)\frac{\partial\tilde{s}}{\partial\xi} = 2\mu\tau_0\omega\xi^2 - 2\mu\epsilon_0 e^{-1/\chi} q(\tilde{s},m;\zeta),$$

$$\tau_0\omega\xi(1-\xi^2)\frac{\partial m}{\partial\xi} = 2q(\tilde{s},m;\zeta)(1-\tilde{s}m),$$

$$\tau_0\omega\xi(1-\xi^2)\frac{\partial\chi}{\partial\xi} = \frac{2\epsilon_0}{c_0\tau_0} e^{-1/\chi}\tilde{s}q(\tilde{s},m;\zeta)(\chi_\infty - \chi). \tag{A3}$$

Also recall that $\dot{R}/R = \omega$. The initial conditions are

$$\tilde{s}(0) = 0, \quad m(0) = 0, \quad \chi(0) = \chi_0. \tag{A4}$$

We have integrated these equations numerically in the limit $\tau_0\omega \to 0$ with $\epsilon_0 = 1$, $c_0 = 1$, $\chi_\infty = 0.13$, $\chi_0 = 0.1$, $\mu/s_y = 50$ and for various values of $\zeta < 10$. Then we have used Eq. (A1) to obtain $\sigma^{\text{th}} \approx 5 s_y$, and have checked that this result is only weakly dependent on ζ.

[1] L. B. Freund, *Dynamic Fracture Mechanics* (Cambridge University Press, Cambridge, 1998).
[2] J. S. Langer, Phys. Rev. E **62**, 1351 (2000).
[3] E. Bouchbinder, A. Pomyalov, and I. Procaccia, Phys. Rev. Lett. **97**, 134301 (2006).
[4] E. Bouchbinder, J. S. Langer, and I. Procaccia, Phys. Rev. E **75**, 036107 (2007).
[5] E. Bouchbinder, J. S. Langer, and I. Procaccia, Phys. Rev. E **75**, 036108 (2007).
[6] M. L. Falk and J. S. Langer, Phys. Rev. E **57**, 7192 (1998); M. L. Falk and J. S. Langer, MRS Bull. **25**, 40 (2000).
[7] J. S. Langer and L. Pechenik, Phys. Rev. E **68**, 061507 (2003).
[8] J. Lubliner, *Plasticity Theory* (Macmillan, New York, 1990).
[9] J. S. Langer and A. E. Lobkovsky, Phys. Rev. E **60**, 6978 (1999).
[10] F. A. McClintock, J. Appl. Mech. **35**, 363 (1968).
[11] J. R. Rice and D. M. Tracey, J. Mech. Phys. Solids **17**, 201 (1969).
[12] M. M. Carroll and A. C. Holt, J. Appl. Phys. **43**, 1626 (1972).
[13] J. N. Johnson, J. Appl. Phys. **52**, 2812 (1981).
[14] S. R. Bodner and Y. Partom, J. Appl. Mech. **39**, 751 (1972).
[15] E. H. Lee, J. Appl. Mech. **36**, 1 (1969).
[16] L. D. Landau and E. M. Lifshitz, *Theory of Elasticity*, 3rd ed. (Pergamon, London, 1986).
[17] J. S. Langer, Phys. Rev. E **70**, 041502 (2004).
[18] Y. Shi, M. B. Katz, H. Li and M. L. Falk, eprint arXiv:cond-mat/0609392 (to be published).